Analysis of the energy harvesting performance of a piezoelectric bender outside its resonance

Adrian Amanci[c], Frédéric Giraud[a,b,*], Christophe Giraud-Audine[a,d], Michel Amberg[a,b], Francis Dawson[c], Betty Lemaire-Semail[a,b]

[a] *Laboratoire d'Electrotechnique et d'Electronique de Puissance*
[b] *University Lille1, Villeneuve d'Ascq Cedex France*
[c] *Dept. of Electrical & Computer Engineering of the University of Toronto, Toronto, Canada*
[d] *École Nationale des Arts & Métier Paris-Tech, Lille, France*

Abstract

When the frequency of the source of vibration of a Piezolectric Generator is significantly different from its eigenfrequency, the dielectric power losses become prominent and decrease the amount of power which is practically harvested. For off-resonance vibrating frequencies, the optimal operating conditions can be obtained with a Maximum Power Point Tracking method. This paper introduces complex phasors in the study of power conversion for piezoelectric generators. These complex phasors are used to describe three strategies which help simplify the tracking of the optimal generator output power for vibration frequencies which are away from resonance. Experimental results obtained on a prototype illustrate and confirm the approach with the phasor approaches illustrate and confirm the success of the proposed optimal power tracking strategies. Finally, we show that the efficiency results of each strategy depend on whether they are used inside or outside a frequency bandwidth around the eigenfrequency, and that the length of this bandwidth depends on the excitation amplitude.

Keywords: Wide-bandwidth, Piezoelectric energy harvester

1. Introduction

Piezoelectric Generators (PEG) are devices which convert power from mechanical vibration into electrical power, the typical extracted power ranging from tens of microwatts to milliwatts [1]. The energy conversion is achieved by using a proof mass attached to a beam which is bent by vibrations and attenuated by the piezoelectric material which is attached to the beam [2]. Because these forces are produced by contact, and not at a distance, the piezoelectric material and the mass have to be coupled, while the piezo electric generator also needs to be firmly attached to a structure [3].

The produced electrical energy cannot be optimally harvested by directly connecting the PEG to the electrical load. With an ideal sinusoidal excitation, an optimal transfer of energy can be obtained if the impedance of the generator matches the impedance of the load [4, 5]. A method of obtaining optimal energy harvesting from a PEG is then to actively modify the equivalent impedance connected to the generator's terminals. For example, authors in [6] have already reported a method to harvest energy at any vibration frequency. Their method consists of using linear and passive elements connected to the piezoelectric generator and adjusting their value to optimize the extracted power from vibrations. However, the method requires a large inductor, and was proposed only for cases where mechanical damping is large. In [7], the authors implement a resistive and inductive impedance matching topology, achieved with a bidirectionnal DC-DC converter and a fixed inductor. They use a 2-D Maximum Power Point Tracking (MPPT) to adjust the duty cycle of the converter, and thus obtain optimal power extraction for a large frequency range.

However, in most practical cases, the electrical load varies with time and it can't be adapted to the generator. This is why, an electrical to electrical energy conversion stage is often included to maximize the power extracted [8], such as *Synchronized Switch Harvesting on Inductor* (SSHI) and *Synchronous Electric Charge Extraction* (SECE). The SSHI technique uses a switched inductor to reverse the voltage across the piezoelectric generator and synchronizes the voltage on maxima and minima of the displacement of the beam [9]. The SECE technique [10] uses a flyback topology to extract the stored electrical energy of the PEG at each maxima of the voltage. With this method, energy extraction is obtained for any load value, and can be used to charge up a battery, in a wireless communication application [11], for example. Both SSHI and SECE are semi-active or semi-passive techniques because the switching command for the controllable switch is obtained from voltage or current level or variation [12].

*Corresponding author

The main issue with semi-active energy conversion techniques is that the harvested power depends on the frequency of excitation. Indeed, the system is a resonant spring-mass system, and the best energy harvesting is obtained at the device's eigenfrequency. To overcome the narrow frequency bandwidth, researchers have proposed many solutions, a classification of which is presented in [13]. Some solutions modify the generator itself, to obtain a non-linear behaviour and increase the frequency bandwidth of the device, without increasing its damping [14]. Other solutions consist of slightly changing the resonant frequency of the system, by introducing an additional force proportional to the displacement with magnets [15], or by using impact-forces [16].

When the power converter fully controls the voltage across the piezoelectric device, the conversion technique is classified as active. As an example, active conversion can be achieved with the help of a Pulse Width Modulation (PWM) and full bridge topology. In the article by Yiming et al. [17], the authors synchronize the voltage to the force applied to the device, while in [18], a controller is designed to maximize the power extracted. In [19], the authors harvest energy by controlling the phase and amplitude of the voltage across the piezoelectric generator, using active energy harvesting. Theoretically, the harvested energy can be maximum even off resonance, but practically, the amount of power is limited by the efficiency of the conversion. The optimal operating conditions, which depend on frequency and voltage amplitude, are obtained using a 2-D MPPT with a two-step gradient-based algorithm. The authors were able to obtain optimal operating conditions after 9 steps and 3 minutes.

Most active energy harvesting techniques make use of a 2D MPPT algorithm in order to extract the largest amount of power from the PEG. A 2D MPPT algorithm is energy and time consuming and requires significant computational power. The purpose of this paper is to simplify this approach, by reducing the dimension of the maximum power point tracking algorithm, as illustrated in Fig. 1.

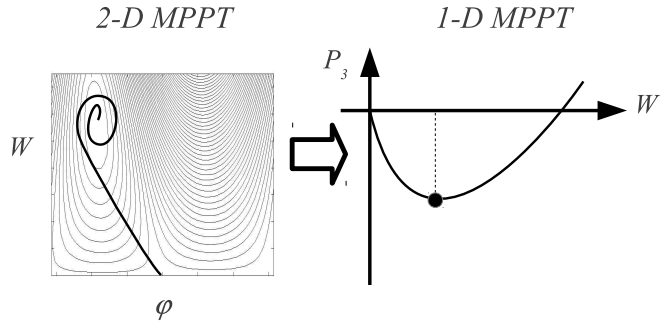

Figure 1: An illustration of a 2-D MPPT where two independent variables are both optimized to attain the maximum output power, and a 1-D MPPT, when one variable is linked to the other.

The outline of the paper is as follows. The second section of the paper establishes the operating conditions required to harvest the maximum mechanical power. The third section confirms these conditions by the experimental tests performed for a narrow frequency bandwidth around the generator's resonance. The last section establishes the optimal operating conditions for a wide operating frequency range for the practical case which includes dielectric losses.

2. Active energy harvesting

2.1. Description of the system

The system shown in Fig. 2 uses a monomorphe, built up with a thin layer of copper on which a layer of piezo material is bonded. A tip mass M is firmly attached at one edge of the device, while the other end is connected to a rigid structure. Vibration of the structure is produced by a shaker, and we denote by z_c the position of the shaker, $\gamma(t) = \ddot{z}_c$ the acceleration, and w the displacement of the tip's mass. From an electrical point of view, the copper plate is connected to ground, and the electrode of the piezoelectric material is set to a potential denoted as v. The current flowing through the electrode is denoted as i.

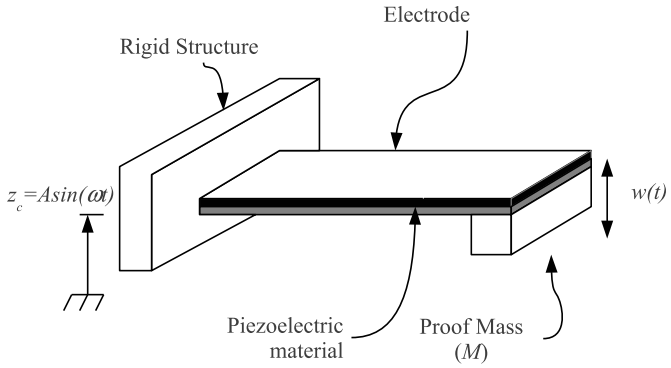

Figure 2: The Piezo-Electric Generator system.

For the formulation presented in this paper, a lossless linear electromechanical conversion is assumed. Moreover, we will consider harmonic excitation at frequencies which are around the first bending mode of the system, while neglecting the contribution of the other bending modes.

2.2. Analytical modelling of the system

The spring-mass system made-up of the mass and the monomorph, can be analytically described by equation 1 [6]:

$$M\ddot{w} + D_s\dot{w} + K_s w = Nv - f_{acc} \tag{1}$$

where w is the displacement of the tip mass with respect to the rigid structure, K_s is the equivalent stiffness of the monomorphe, D_s is the equivalent damping, and N is a force conversion factor. The force f_{acc} is an inertial force acting on the mass, and it is equal to:

$$f_{acc} = M\ddot{z}_c \tag{2}$$

In this paper, we assume monochromatic excitations, where $\gamma(t)$ and the tip's displacement $w(t)$ are sinusoidal functions of time; if the time reference is set on the excitation, we can write:

$$\ddot{z}_c = \Gamma sin(\omega t) \quad (3)$$
$$w = W sin(\omega t - \varphi) \quad (4)$$

For the purpose of clarity, we introduce the complex notation of $x(t)$: $x(t) = Im(\underline{x})$ with $\underline{x} = \underline{X}e^{j\omega t}$, $j^2 = -1$, and $Im(\underline{x})$ is the imaginary part of $\underline{x}$. The complex notation provides the following phasor representations of the tip's displacement $\underline{W}$, the voltage $\underline{V}$ and the acceleration force $\underline{F}_{acc}$ as follows:

$$\begin{aligned} \underline{F}_{acc} = F_{acc} = M\Gamma \\ \underline{W} = We^{-j\varphi} \\ \underline{V} = Ve^{-j\delta} \end{aligned} \quad (5)$$

Rewriting equation 1 in phasor form leads to:

$$(K_s - M\omega^2)\underline{W} + jD_s\omega\underline{W} = N\underline{V} - \underline{F}_{acc} \quad (6)$$

The operating point of the PEG, which is determined by phasors $\underline{V}$, $\underline{W}$, $\underline{F}_{acc}$ and the operating frequency ω, can be represented by the phasor diagram in Fig. 3. In this representation, phasors are vectors in the complex plane, and the position of the phasors satisfies equation 6. We also introduce $\psi = \varphi - \delta$, the phase of $\underline{V}$ with respect to $\underline{W}$.

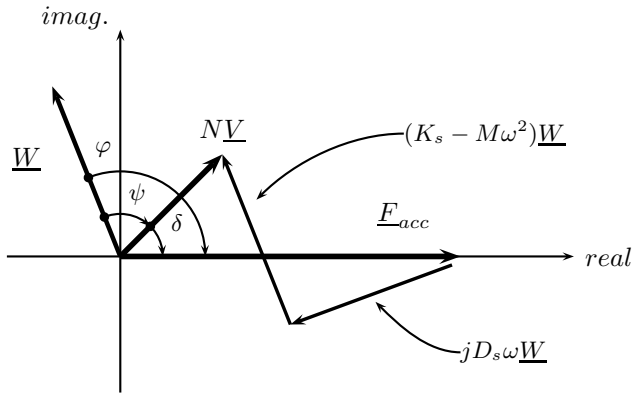

Figure 3: Complex phasors representation of an operating point.

The energy converted to an electrical form is extracted from the kinetic energy of the mass [20]. The mechanical power extracted from the PEG is computed with the help of equations 2 and 5 and is provided next:

$$\begin{aligned} P_1 &= \frac{1}{2}Re(\underline{f}_{acc}\underline{\dot{w}}^*) \\ &= \frac{1}{2}Re(M\Gamma e^{j\omega t} \cdot (-j)\omega W e^{-j(\omega t - \varphi)}) \\ &= \frac{1}{2}M\Gamma\omega W sin(\varphi) \end{aligned} \quad (7)$$

Hence, the power extracted from the proof mass depends on the displacement amplitude W, on the amplitude of the acceleration Γ, and on the phase shift φ. In other words, it is the projection of $\underline{W}$ on the imaginary axis which is important for the realization of energy harvesting.

However, the mechanical power losses, which are responsible for damping the amplitude of the bender vibration, reduce the amount of harvested power. We approximate these losses with the help of equation 8:

$$P_m = \frac{1}{2}D_s(\omega W)^2 \quad (8)$$

The power P_2 which is converted into usable electrical power is then given by:

$$\begin{aligned} P_2 &= P_1 + P_m \\ &= \frac{1}{2}M\Gamma\omega W sin(\varphi) + \frac{1}{2}D_s(\omega W)^2 \end{aligned} \quad (9)$$

In equation 7, more power is extracted if W is increased, but equation 8 shows that we also have more mechanical losses: to harvest more power from the proof mass, we first have to maximize P_1 for a given value of W. This is achieved if:

$$\varphi = -\frac{\pi}{2} \quad (10)$$

Moreover, [6] shows that there exists an optimal displacement W which optimizes P_2. The optimal displacement magnitude is obtained by solving the following equation for W:

$$\left.\frac{\partial P_2}{\partial W}\right|_{W_{opt}} = 0. \quad (11)$$

This gives rise to the following equation, when $\varphi = -\frac{\pi}{2}$:

$$-\frac{1}{2}M\Gamma\omega + D_s\omega^2 W_{opt} = 0 \quad (12)$$

yielding:

$$W_{opt} = \frac{M\Gamma}{2D_s\omega} \quad (13)$$

Under this condition, the optimal output power is given by:

$$P_{2opt} = -\frac{(M\Gamma)^2}{8D_s} \quad (14)$$

In addition to the mechanical power losses, the dielectric power losses P_d also reduce the amount of power which can be practically harvested [21]. The electrical power harvested is then given by:

$$P_3 = P_2 + P_d \quad (15)$$

In this condition, harvesting the maximum of energy requires a 2-D Maximum Power Point Tracking optimization loop as in [19], where the voltage amplitude and phase are slightly changed to attain this optimum. This process needs computation effort and thus energy. The next section of the paper presents strategies to simplify the optimization loop, at the expense of lower amount of harvested energy.

3. Strategies

The strategies presented in this section fix one phase shift, while one variable has to be optimized through a MPPT loop. The three strategies presented in this paper are denoted as (1) *In-Phase*, (2) *Optimal mechanical energy harvesting* and (3) *Lower voltage*. With the *In-phase* and *Optimal mechanical power* strategies, the vibration amplitude is used to obtain the maximal harvested power, while with the *Lower voltage strategy* the voltage amplitude is altered in order to improve the PEG harvested energy.

3.1. In-Phase strategy

In the *In-phase* strategy, the voltage is set in phase with the displacement speed $\dot{w}$ [22], or, equivalently, in quadrature to the displacement w. This leads to $\psi = -\frac{\pi}{2}$ which results in:

$$\varphi = -\frac{\pi}{2} + \delta \tag{16}$$

It is possible to demonstrate that this is optimal when operating at the eigenfrequency of the bender. Indeed, at the system's resonance frequency, the term $(K_s - M\omega^2)$ equals zero, which leads to the following revision of equation 6:

$$jD_s\omega W e^{-j\varphi} = NVe^{-j\delta} - \underline{F}_{acc} \tag{17}$$

Substituting 16 into 17, and multiplying the left and right hand side by $e^{-j\delta}$ leads to:

$$-D_s\omega W = NV - \underline{F}_{acc}e^{j\delta} \tag{18}$$

Because the left and right members of this equation is a real number, $e^{j\delta}$ is also real, leading to $\delta = \{0; \pi\}$. The case $\delta = \pi$ condition doesn't correspond to a case of energy harvesting, so it will be disregarded. The condition $\delta = 0$ requires $\varphi = \frac{\pi}{2}$. This condition can be represented using complex phasors as shown in Fig. 4.

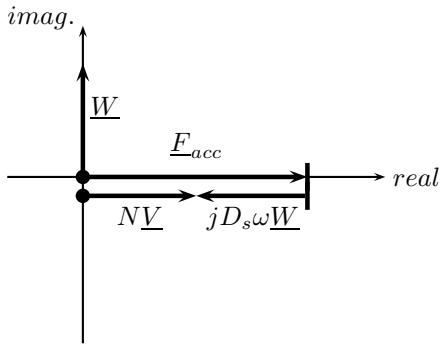

Figure 4: Complex phasors representation at resonance.

With the *In-phase* strategy, conditioning circuits associated with techniques like the *Synchronous Charge Extraction* [23] can attain the optimal operating conditions at any load value. However, Fig. 4 and equation 16 are only valid at resonance, and using $\psi = -\frac{\pi}{2}$ below or above resonance does not provide optimal power extraction from the PEG. The next section deals with the optimal operating conditions in the vicinity of the bender's resonant frequency.

3.2. Optimal mechanical energy harvesting $\varphi = -\frac{\pi}{2}$

If the vibration's frequency ω shifts away from the bender resonant frequency, energy harvesting can still occur and the optimal conditions introduced in equations 10 and 13 still lead to the optimal power harvested from the proof mass.

However, to obtain $\varphi = -\frac{\pi}{2}$, the operating conditions have to be changed compared to the *In-phase* strategy. For, $(K_s - M\omega^2) \neq 0$, the phasor representation is shown in Fig. 5; in this figure we compare two cases, for ω below or above the resonant frequency of the bender.

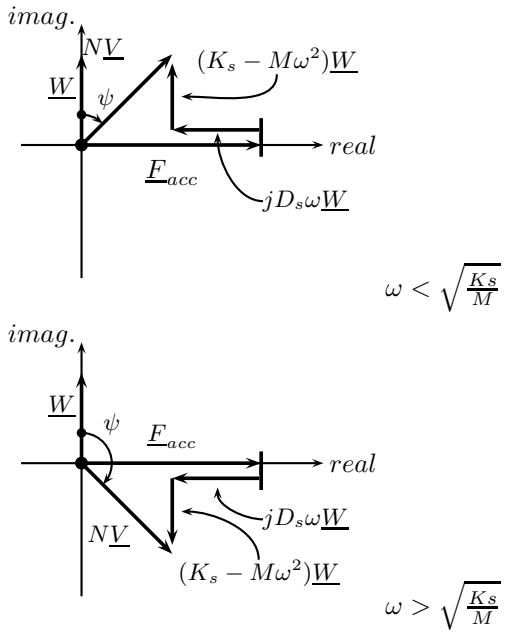

Figure 5: Complex phasors representation for the optimal mechanical harvested energy P_2.

With the *In-phase* strategy, the voltage phase is set at $\frac{\pi}{2}$ with respect to the phase of the mechanical displacement $\underline{W}$. However, for converter operation above or below resonance, the optimal required angle difference changes. The optimal angle ψ between $\underline{V}$ and $\underline{W}$ can be calculated as:

$$\begin{aligned} \psi &= -\frac{\pi}{2} + \arctan\frac{(K_s - M\omega^2)W}{F_{acc} - D_s\omega W} \\ &= -\arctan\frac{F_{acc} - D_s\omega}{(K_s - M\omega^2)} \end{aligned} \tag{19}$$

The evolution of ψ as a function of ω is depicted in Fig. 6.

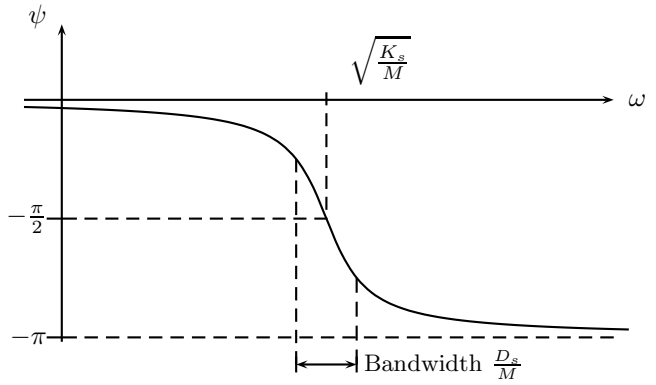

Figure 6: Phase of the voltage compared to the tip's displacement as a function of ω.

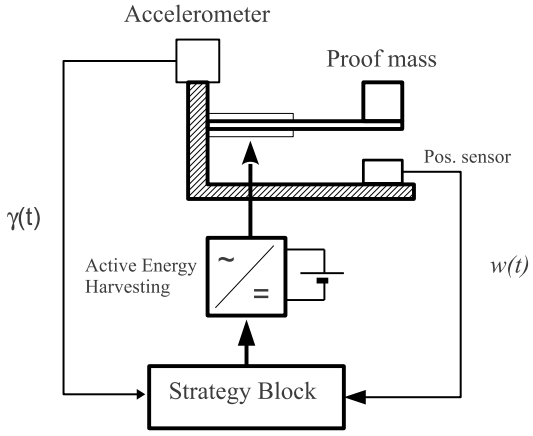

Figure 7: Presentation of the closed loop control.

Hence, in the vicinity of the resonant frequency of the PEG, and more particularly within the frequency bandwidth, the phase shift ψ between the voltage v and the displacement w is not constant and varies from $-\pi$ to 0. Moreover, for a vibration frequency outside the frequency bandwidth, ψ changes very little, and is approximately equal to $-\pi$ above the resonant frequency, and 0 below it. Note that even far away from resonance, the optimal mechanical power extracted remains the same, and the extracted power would not change assuming no power losses.

To adapt the phase shift ψ based on the frequency ω, one could estimate the apropriate value of $\psi(\omega)$ and fine tune this value with a voltage source. However, this seems difficult and impractical, since the resonant frequency may change with temperature [24].

This is why a closed loop control, as presented in Fig. 7, could be used instead of open loop tuning of the system. From the measurement of the case's acceleration $\gamma(t)$, a reference for $\underline{W}$ is determined by the strategy block: its phase is phase shifted by $-\frac{\pi}{2}$ compared to $\gamma(t)$ and its amplitude is calculated from the optimal conditions presented in equation 13. The strategy block also computes the voltage references needed to obtain the required vibration, which is produced by the DC to AC active energy circuit.

3.3. Lower voltage strategy $\delta = \pm\frac{\pi}{2}$

For operation below or above the bender's resonant frequency, optimal mechanical energy harvesting is obtained at the expense of higher voltage amplitude V. However, this leads to higher dielectric power losses in the material. To reduce these power losses and thus increase the efficiency of the conversion, other piezoelectric generator structures can be considered, as in [25, 26]. It is also possible to change the control strategy, and to harvest less mechanical power for a given vibration amplitude W, provided that it leads to lower voltage amplitude V, and thus, lower dielectric losses. To detail this point, let us consider the phasor representations shown in Fig. 8. This figure shows two operating conditions. The first one (Fig. 8(a)) represents the optimal mechanical energy harvesting point, and thus $\varphi = -\frac{\pi}{2}$. In the second phasor representation presented in (Fig. 8(b)), φ and W are set so as to keep $Im(\underline{W})$ unchanged with respect to Fig. 8(a), that is the mechanical power in both cases is equal. However, since V is decreased, the dielectric losses are reduced.

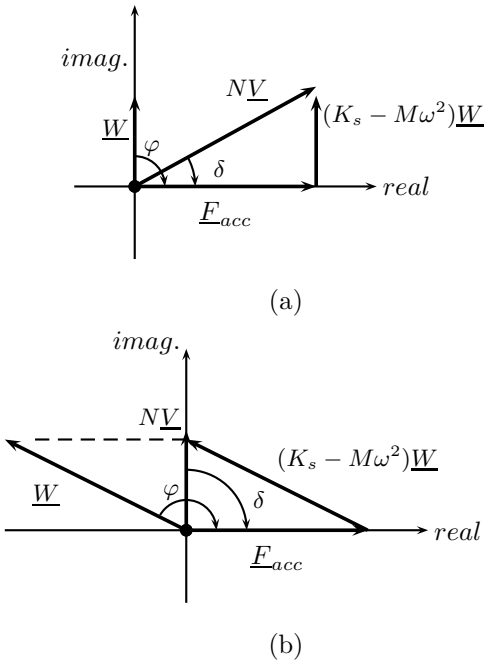

Figure 8: Complex phasors representations with $\omega < \sqrt{\frac{K_s}{M}}$; (a) for the optimal mechanical harvested energy P_2, (b) for $\delta = -\frac{\pi}{2}$.

If this method is used outside the generators bandwidth, we consider that $|K_s - M\omega^2| \gg D_s\omega$. With this assumption, equation 6 can be written as:

$$\left(K_s - M\omega^2\right)\underline{W} = N\underline{V} - F_{acc} \tag{20}$$

In order to reduce the magnitude of V while maintaining the same mechanical power (assuming $W\sin(\varphi)$ is

constant), the real power of V should equal 0, as depicted in Fig. 8. Hence, for a vibration frequency far away from the eigenfrequency, the voltage should be phase shifted by $\frac{\pi}{2}$ (if $\omega \ll \sqrt{\frac{K_s}{M}}$) or $-\frac{\pi}{2}$ (if $\omega \gg \sqrt{\frac{K_s}{M}}$), in order to have lower voltage amplitude V, and thus, less dielectric power losses.

In the next section, a series of experimental tests are presented to evaluate the three strategies introduced in this section.

4. Experimental study

4.1. Model validation

The modelling of section 2.1 is compared to actual measurements on the device presented in Fig. 9. The layer of piezoelectric material is built up with four rectangles made of NCE41, a material from Noliac. The proof mass is built up with an accumulation of brass deposited on the layer of copper, and a small mirror and magnet are added to the tip, in order to measure $w(t)$.

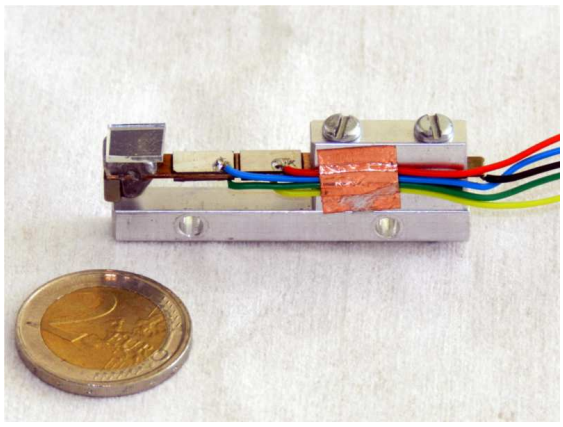

Figure 9: Presentation of the experimental system.

During the experimental trials performed, the bender is shaken with a LDS V406 industrial shaker from Bruël & Kjaer. Measurements of $\gamma(t)$ are obtained with an accelerometer, measurements of $v(t)$ with a Tektronix P3010 voltage probe and $i(t)$ with a Tektronix TCP202 Current probe. With the measurements introduced above, we post process the following:

- Γ, W, V which are the amplitude values of $\gamma(t)$, $w(t)$ and $v(t)$ respectively,
- the power converted into electricity within the bender P_2 using the hysteresis loop (w, f_p)
- the power harvested at the electrical terminal P_3 using $v(t)$ and $i(t)$, taking into account the power of the equivalent $10M\Omega$ resistor of the voltage probe.

The parameters of the bender were identified from the system's response to a voltage step and are provided in Table 1.

Table 1: Parameters of the experimental system.

M	$1,92g$
D_s	$0,05Ns/m$
K_s	$2169N/m$
N	$0,185mN/V$
C_b	$2,93nF$
1^{st} bending mode	$169Hz$

4.2. Power harvesting in the vicinity of resonance

In this study, we want to confirm the analytical results of section 3. For that purpose, we first perform a test at the bender's resonance frequency. For the test, we have $\Gamma = 5m/s^2$, and we control v in order to obtain W constant and equal to $W = 40\mu m$, and $-\pi < \varphi < \pi$. The results are presented in Fig. 10.

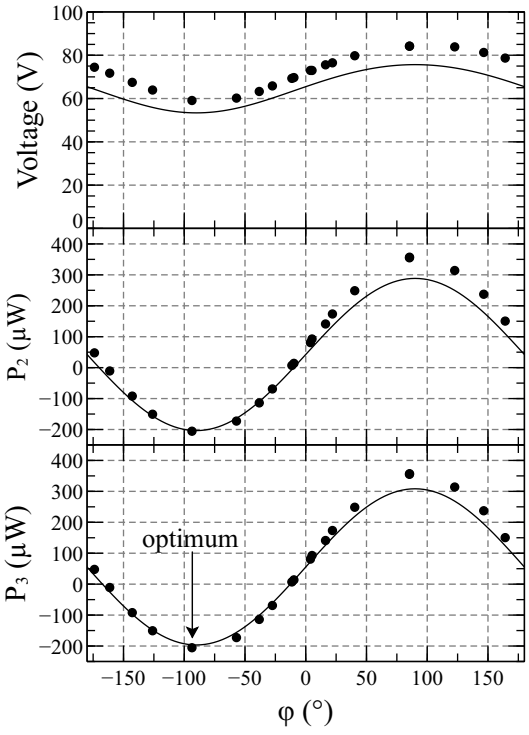

Figure 10: V, P_2, and P_3 as a function of the phase shift φ at resonance with $\Gamma = 5.5m/sec^2$ and $W = 40\mu m$; •: experimental, -: model.

The experimental results are compared to the model, and they are in a good agreement. It shows that P_2 depends on φ and follows the same sinusoidal profile as P_1 in equation 7. The amplitude of P_2 is equal to $\frac{1}{2}M\Gamma\omega W$, which holds for all of the operating points; the bias of P_2 is given by P_m which is also constant.

Experimentally, we check that the condition $\varphi = -\frac{\pi}{2}$ corresponds to the maximal power harvested from the device, *i.e.* P_2 is minimal. For $\varphi = -\frac{\pi}{2}$, the power is shared as follows:

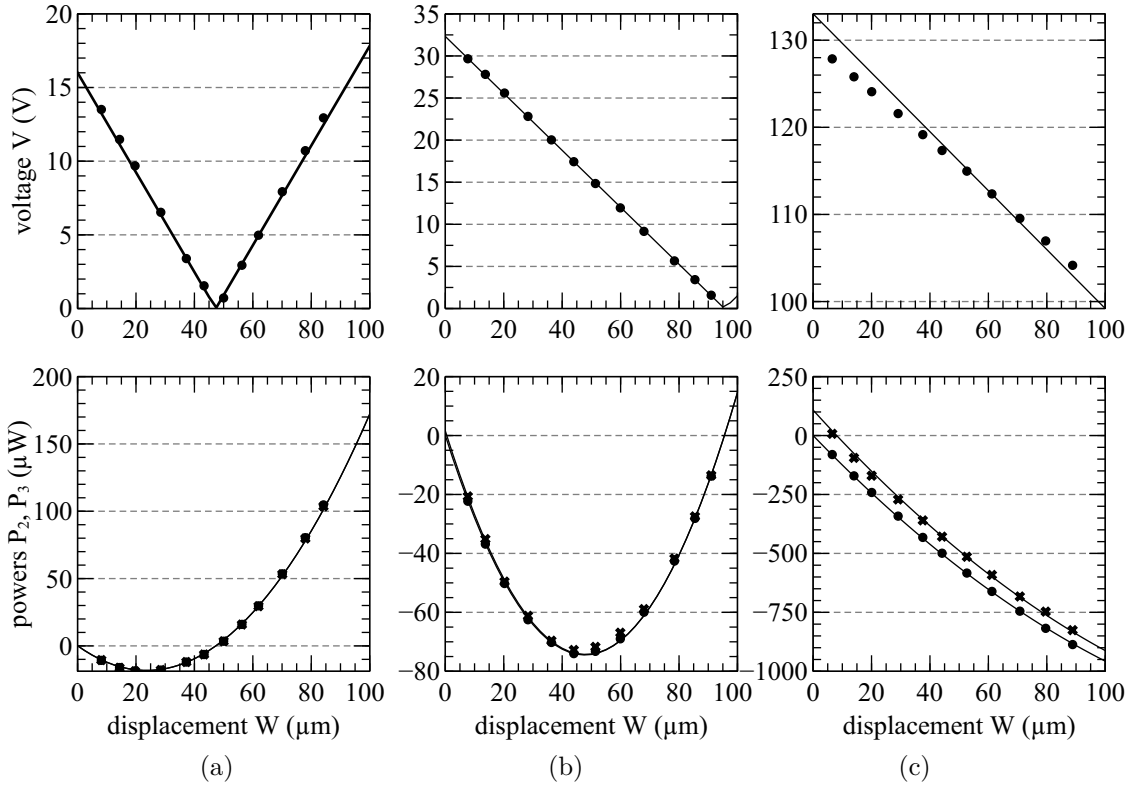

Figure 11: Voltage amplitude V, mechanical Power P_2 (•)and electrical power P_3 (×), as a function of the displacement W at resonance, $\varphi = -\frac{\pi}{2}$; (a) $\Gamma = 1m/sec^2$, (b) $\Gamma = 2.5m/sec^2$; (c) $\Gamma = 10m/sec^2$ •: experimental, -: model.

- the proof mass produces $P_1 = 243\mu W$,
- the power converted into electrical power is equal to $P_2 = 200\mu W$,
- losses are equal to $P_m = 43\mu W$ for the mechanical losses, and $P_d = 12\mu W$ for the dielectric losses.

If W varies and φ is kept constant and equal to $-\frac{\pi}{2}$, the harvested power P_2 follows a parabolic curve, as shown experimentally in Fig. 11.

The value found for the optimal displacement W_{opt} is in good agreement with theory at resonance; for example, we calculate $W_{opt} = 22\mu m$ and we measure $20\mu m$ at $1m/sec^2$. Moreover, the curves P_2 and P_3 are very similar for each case of vibration acceleration level selected. Indeed, at the optimal operating point, the dielectric power losses are small compared to the mechanical power losses. For example, for $\Gamma = 1m/sec^2$, we calculate $P_m = 17\mu W$ and $P_d < 1\mu W$.

Finally, we also checked that the voltage's phase was equal to 0 with respect to $\underline{F_{acc}}$, which confirms the property of the *In-phase* strategy to operate at the optimal phase conditions.

Figure 12 presents one result when the vibration frequency moves away from resonance $(165Hz)$, for $\Gamma = 2m/sec^2$.

The optimal power still occurs at $\varphi = -\frac{\pi}{2}$, and the computed optimal displacement amplitude ($W_{opt} = 40\mu m$)

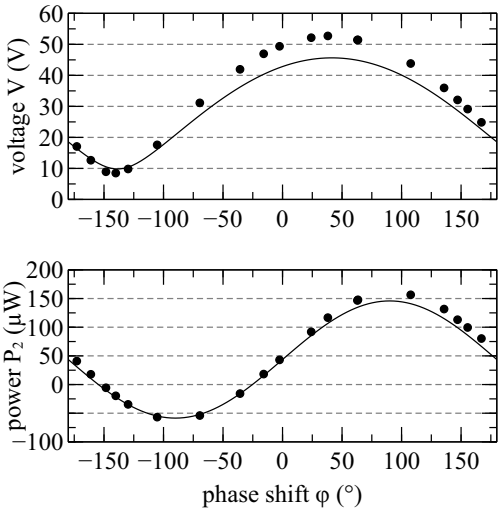

Figure 12: P_2 and V as a function of the phase shift φ at $165Hz$, $W = 40\mu m$ and $\Gamma = 2m/sec^2$; •: experimental, –: model.

is confirmed by Fig. 13, which displays P_2 as a function of W for $\varphi = -\frac{\pi}{2}$.

As previously established by equations 19 and Fig. 5, the phase shift of the voltage δ is not equal to 0 for this optimal condition. Fig. 14 presents δ as a function of φ for $W = W_{opt}$ and $\Gamma = 2m/sec^2$. We measured $\delta = -40deg$ for the optimal operating condition. For the *In-phase*

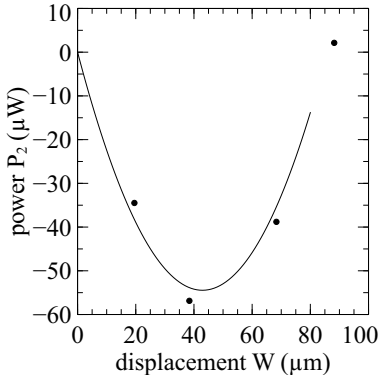

Figure 13: Mechanical Power P_2, as a function of the displacement W at $165Hz$, $\varphi = -\frac{\pi}{2}$ and $\Gamma = 2m/sec^2$; •: experimental, –: model.

strategy, the condition imposed by equation 16 is exemplified in Fig. 14, with $\delta = -28deg$ and $\varphi = 118deg$. This highlights the fact that the condition imposed by equation 10 cannot be obtained outside resonance with the *In-phase* strategy.

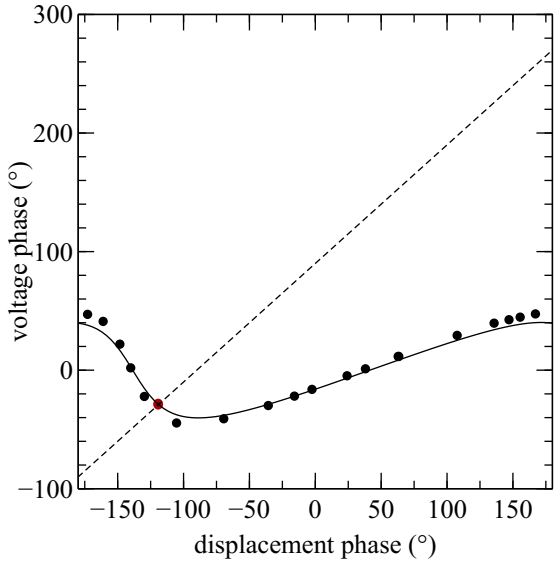

Figure 14: Angle δ as a function of φ for $W = 40\mu m$ at $165Hz$ and $\Gamma = 2m/sec^2$; •: experimental, -: model, –: $\delta = \varphi + \frac{\pi}{2}$

The results presented in this section were obtained in the vicinity of the eigenfrequency of the bender, where the voltage across the bender's terminals is not very high. If we shift away from resonance more, the voltage amplitude increases, leading to higher dielectric losses. The next section deals with this particular case.

4.3. Optimal energy harvesting outside resonance

At excitation frequencies outside of the bender's bandwidth, the required voltage to operate at the optimal displacement can be large. This is due to the term $K_s - M\omega^2$, which becomes prominent and can be very large compared to $D_s\omega$. For example, in our experimental system, large voltages are developed at $10Hz$ away from the system's resonance.

For this type of operating condition, higher voltage is needed to obtain the same displacement amplitude. For example, Fig. 15 shows an experimental test at $180Hz$ and $40\mu m$ with $\Gamma = 2m/sec^2$.

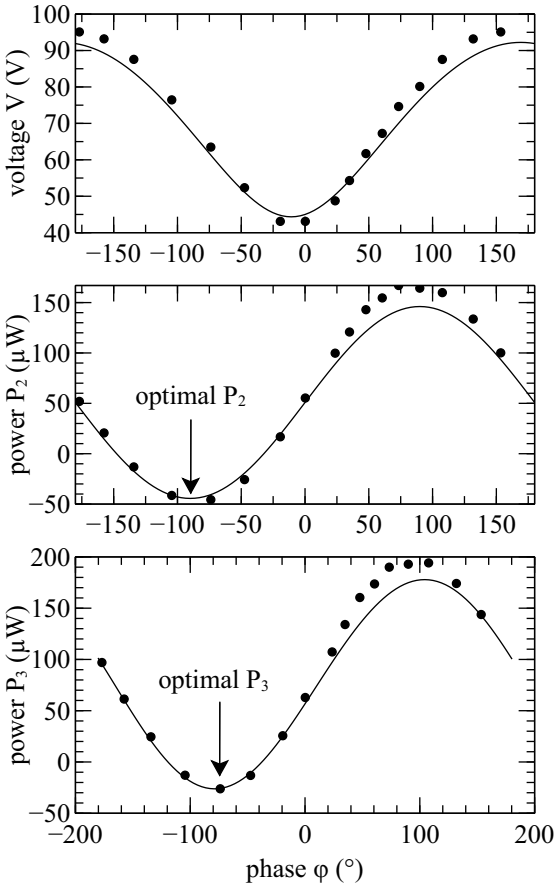

Figure 15: Voltage amplitude V, mechanical power P_2 and electric power P_3, as a function of the angle φ at $180Hz$, $W = 40\mu m$ and $\Gamma = 2m/sec^2$; •: experimental, -: model.

The required voltage is approximately $68V$, as opposed to the $20V$ at $165Hz$, but mechanical power is still optimally extracted when $\varphi = -\frac{\pi}{2}$. Hence, even at frequencies outside the bender's bandwidth, equations 10 and 13 still lead to optimal mechanical power generated. For $\omega = 180Hz$, the power is shared as follows: $P_1 = -92\mu W$, $P_m = 50\mu W$ and $P_d = 20\mu W$.

However, the optimal power P_3 is obtained for $\varphi = -72deg$. This is due to the dielectric power losses which have increased considerably, and can no longer be neglected. It may therefore be better to operate at a different point other than the theoretically optimal condition (which ignores dielectric losses). Indeed, by allowing a non-optimal phase shift of the displacement $\underline{W}$, V decreases. Of course, P_1 is increased for the same level of displacement amplitude W; but P_d is decreased and the global power is lower. At $\varphi = -72deg$, the power is shared

as follows: $P_1 = -90\mu W$, $P_m = 50\mu W$ and $P_d = 14\mu W$.

To obtain the optimal operating conditions while accounting for dielectric losses, we have to introduce $\underline{W} = We^{-j\varphi}$ into equations 6, 7, 8 in order to find the optimal values of φ and W. This can be done numerically, and practically with an optimization loop as in [19].

5. Discussion

5.1. Influence of the strategy

Fig. 16 displays the power components P_2 and P_3 as a function of frequency $f = \frac{\omega}{2\pi}$ that can be extracted from the PEG. When the displacement $w(t)$ is controlled, both in amplitude and in phase compared to the acceleration $\gamma(t)$, the theoretical power P_2 is constant and no longer depends on the frequency, while the electrically extracted power P_3 drops to zero due to the large dielectric power losses generated.

This optimal power is compared to the results obtained with each strategy presented in section 3. The *In-phase* strategy, which consists in setting the voltage $\underline{V}$ phase shifted by $\frac{\pi}{2}$ compared to the displacement $\underline{W}$ is optimal at resonance, but non optimal outside resonance. The power produced with the *In-phase* strategy is maximal at bender's resonance, and the amount of power which is harvested dramatically drops to zero as the frequency shifts away from resonance.

With the second introduced strategy, denoted as the *optimal mechanical energy harvesting strategy*, we control W such that $\varphi = -\frac{\pi}{2}$, and we are able to harvest close to optimal power, but in a limited bandwidth around resonance.

The third strategy denoted as the *lower voltage strategy*, where a lower value of V is obtained by setting $\delta = \pm\frac{\pi}{2}$, is not efficient at resonance. However, for operation outside of the PEG frequency bandwidth, this strategy allows for close to optimal optimal power extraction.

Hence, to achieve energy harvesting over a broad frequency range, the displacement W has to be controlled both in amplitude and in phase, with $\varphi = -\frac{\pi}{2}$ in the vicinity of the eigenfrequency. For operation further away from resonance, the lower voltage strategy provides close to optimal energy harvesting.

Fig. 16 suggests that using one strategy at a time, either the *Optimal mechanical energy harvesting strategy* close to resonance or the *Lower voltage strategy* further away from resonance, allows for close to optimal power extraction. By alternating between these two strategies based on the vibrating frequency, the optimization strategy is simplified when compared to a 2D-MPPT algorithm. Rather than performing a simultaneous optimization on two variables, only one variable has to be tuned (either W or V) with the proposed strategies.

This conclusion also holds true for large vibration amplitude Γ. This is illustrated by Fig. 17 where $\Gamma = 10m/s^2$.

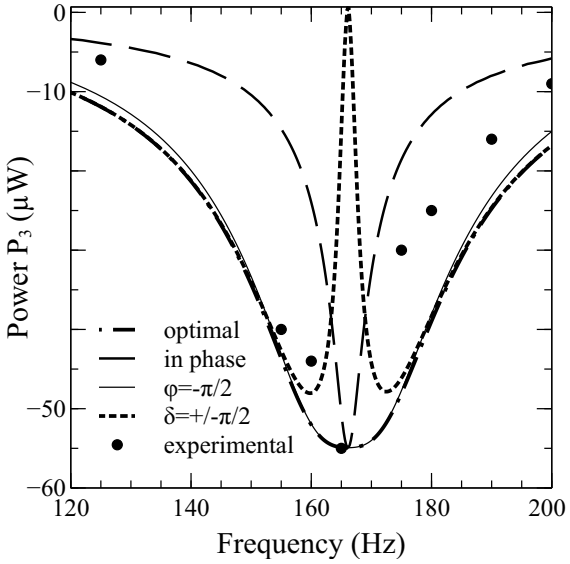

Figure 16: Electric power P_3 for $\Gamma = 2m/sec^2$, as a function of the frequency $f = \frac{\omega}{2\pi}$; ·− optimal operating conditions; −− *In-phase* strategy, − *Maximal mechanical power* strategy, - - *Lower voltage* strategy,•: experimental.

However, the frequency at which one strategy becomes better than the other has changed from approximately $26Hz$ at $\Gamma = 2m/sec^2$ to approximately $16Hz$ at $\Gamma = 10m/sec^2$. The analysis of this corner frequency is given in the next section of the paper.

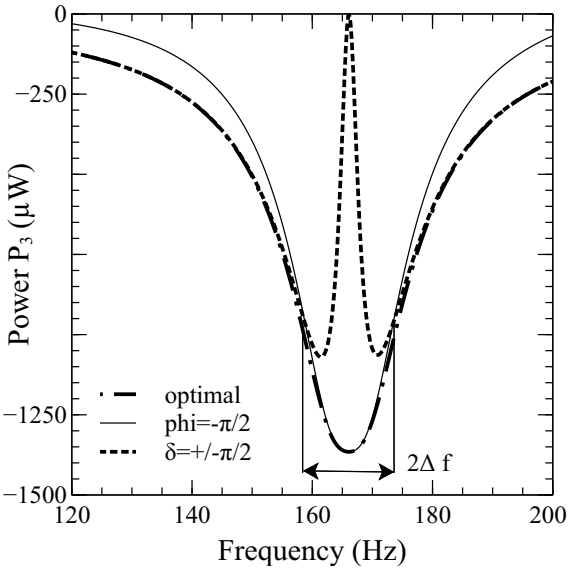

Figure 17: Electric power P_3 for $\Gamma = 10m/sec^2$, as a function of the frequency $f = \frac{\omega}{2\pi}$; ·− optimal operating conditions; − *optimal mechanical power strategy*, - - *Lower voltage* strategy.

5.2. Determination of the corner frequency shift

There are two frequencies ($f_{res} + \Delta f$ and $f_{res} - \Delta f$ where f_{res} is the resonant frequency) for which the *lower voltage strategy* produces the same harvested power as the

Optimal mechanical power strategy. Fig. 18 shows the evolution of Δf as a function of the level of vibration Γ.

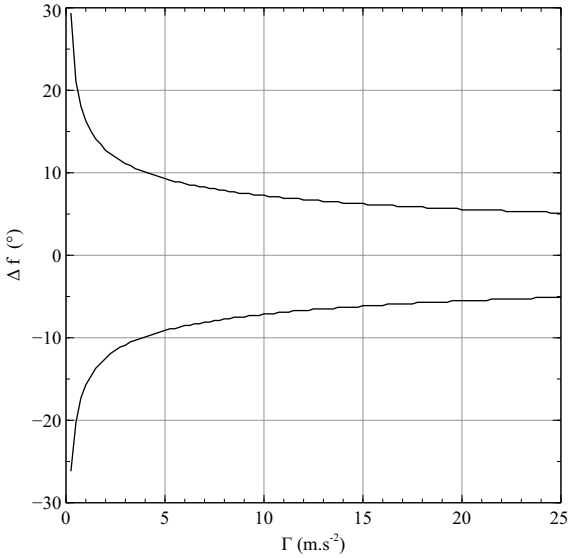

Figure 18: Δf as a function of Γ for the prototype; simulation results.

The results show that for low vibration acceleration, the frequency shift is high, which suggests that the *Optimal mechanical power strategy* can be used over a large frequency span. Is the vibration acceleration amplitude is increased, the Δf decreases, which reduces the frequency band for which the *Optimal mechanical power strategy* is viable. If a larger operating frequency span is needed, the PEG-converter setup should switch between the *Optimal mechanical power strategy* and the *lower voltage strategy* at the appropriate frequencies ($f_{res} + \Delta f$ and $f_{res} - \Delta f$) in order to harvest more power. For example, with our setup, this could arise for a frequency shift of $26Hz$ at $\Gamma = 2m/sec^2$ and $10Hz$ at $\Gamma = 25m/sec^2$.

6. Conclusion

This paper describes power conversion in a PEG. We show that even outside the bender's bandwidth, the optimal operating condition leading to the maximum harvested power leads to the control of the tip's displacement in amplitude and in phase relative to the structure's vibrations. We also show that theoretically, this condition doesn't depend on frequency. This result, which is confirmed by other studies, is presented here by using complex phasor notation.

Practically, the dielectric power losses reduce the amount of power actually harvested, but the same optimal conditions still exist in a narrow bandwidth around resonance. However, for a large frequency span, the dielectric power losses change the operating conditions and a 2-D Maximum Power Point Tracking algorithm has been previously introduced and used to track the optimal operating conditions.

In this work, we propose to control either the voltage or the displacement, depending on the vibrating frequency. For a vibrating frequency around resonance ($f_{res} - \Delta f < f < f_{res} + \Delta f$), we employ the *Optimal mechanical power strategy* and just control the displacement, while for operating frequencies outside of resonance ($f < f_{res} - \Delta f$ or $f > f_{res} + \Delta_f$), we employ the *lower voltage strategy* and just control the voltage. This tuning of a single variable (either voltage or displacement) allows for the implementation of a 1-D MPPT algorithm, as opposed to a 2-D MPPT algorithm which was previously proposed.

In our experimental test bench, an accelerometer was set up in order to measure $\gamma(t)$. The power consumption of this sensor was not taken into account in the global energy sharing of the system. We show that controlling the tip's displacement $w(t)$ in quadrature with the acceleration allows to obtain a good approximation of the optimal power, provided that the excitation frequency doesn't shift more that a threshold.

Acknowledgement

This work has been carried out within the IRCICA Stimtac Project, and the INRIA Mint Project.

7. References

[1] D. Guyomar, M. Lallart, Recent progress in piezoelectric conversion and energy harvesting using nonlinear electronic interfaces and issues in small scale implementation, Micromachines 2 (2) (2011) 274–294.

[2] H. Shen, J. Qiu, M. Balsi, Vibration damping as a result of piezoelectric energy harvesting, Sensors and Actuators A: Physical 169 (1) (2011) 178 – 186.

[3] C. J. Rupp, A. Evgrafov, K. Maute, M. L. Dunn, Design of piezoelectric energy harvesting systems: A topology optimization approach based on multilayer plates and shells, Journal of Intelligent Material Systems and Structures 20 (16) (2009) 1923–1939.

[4] J. Lian, W.-H. Liao, Impedance matching for improving piezoelectric energy harvesting systems, in: Proc. SPIE 7643, Active and Passive Smart Structures and Integrated Systems 2010, 2010, pp. 1–12.

[5] H. Kim, S. Priya, H. Stephanou, K. Uchino, Consideration of impedance matching techniques for efficient piezoelectric energy harvesting, Ultrasonics, Ferroelectrics and Frequency Control, IEEE Transactions on 54 (9) (2007) 1851–1859.

[6] M. J. Renno, F. M. Daqaq, J. I. Daniel, On the optimal energy harvesting from a vibration source, Journal of Sound and Vibration 320 (1–2) (2009) 386 – 405.

[7] S. Saggini, S. Giro, F. Ongaro, P. Mattavelli, Implementation of reactive and resistive load matching for optimal energy harvesting from piezoelectric generators, in: Control and Modeling for Power Electronics (COMPEL), 2010 IEEE 12th Workshop on, 2010, pp. 1–6.

[8] G. Szarka, B. Stark, S. Burrow, Review of power conditioning for kinetic energy harvesting systems, Power Electronics, IEEE Transactions on 27 (2) (2012) 803–815.

[9] D. Guyomar, A. Badel, E. Lefeuvre, C. Richard, Toward energy harvesting using active materials and conversion improvement by nonlinear processing, Ultrasonics, Ferroelectrics and Frequency Control, IEEE Transactions on 52 (4) (2005) 584–595.

[10] E. Lefeuvre, A. Badel, C. Richard, L. Petit, D. Guyomar, A comparison between several vibration-powered piezoelectric generators for standalone systems, Sensors and Actuators A: Physical 126 (2) (2006) 405 – 416.

[11] Y. Tan, J. Y. Lee, S. Panda, Maximize piezoelectric energy harvesting using synchronous charge extraction technique for powering autonomous wireless transmitter, in: IEEE International Conference on Sustainable Energy Technologies, 2008, pp. 1123–1128.

[12] A. Badel, G. Sebald, D. Guyomar, M. Lallart, E. Lefeuvre, C. Richard, J. Qiu, Piezoelectric vibration control by synchronized switching on adaptive voltage sources: Towards wideband semi-active damping, J. Acoust. Soc. Am 119 (5) (2006) 2815–2825.

[13] J. Twiefel, H. Westermann, Survey on broadband techniques for vibration energy harvesting, Journal of Intelligent Material Systems and Structures 24 (11) (2013) 1291–1302.

[14] H. Liu, C. Lee, T. Kobayashi, C. J. Tay, C. Quan, Piezoelectric mems-based wideband energy harvesting systems using a frequency-up-conversion cantilever stopper, Sensors and Actuators A: Physical 186 (2012) 242 – 248.

[15] M. Ferrari, V. Ferrari, M. Guizzetti, B. Andò, S. Baglio, C. Trigona, Improved energy harvesting from wideband vibrations by nonlinear piezoelectric converters, Sensors and Actuators A: Physical 162 (2) (2010) 425 – 431, eurosensors XXIII, 2009.

[16] M. A. Halim, J. Y. Park, Theoretical modeling and analysis of mechanical impact driven and frequency up-converted piezoelectric energy harvester for low-frequency and wide-bandwidth operation, Sensors and Actuators A: Physical 208 (2014) 56 – 65.

[17] L. Yiming, T. Geng, W. Yong, L. Junhong, Z. Qiming, H. F. Hofmann, Active piezoelectric energy harvesting: General principle and experimental demonstration, Journal of Intelligent Material Systems and Structures 20 (5) (2009) 575–585.

[18] J. T. Scruggs, I. L. Cassidy, S. Behrens, Multi-objective optimal control of vibratory energy harvesting systems, Journal of Intelligent Material Systems and Structures 23 (18) (2012) 2077–2093.

[19] C. Luo, H. Hofmann, Wideband energy harvesting for piezoelectric devices with linear resonant behavior, Ultrasonics, Ferroelectrics and Frequency Control, IEEE Transactions on 58 (7) (2011) 1294–1301.

[20] C. Williams, R. Yates, Analysis of a micro-electric generator for microsystems, Sensors and Actuators A: Physical 52 (1–3) (1996) 8 – 11.

[21] J. Liang, W. Liao, On the influence of transducer internal loss in piezoelectric energy harvesting with sshi interface, Journal of Intelligent Material Systems and Structures 22 (5) (2011) 503–512.

[22] Y. C. Shu, I. C. Lien, W. J. Wu, An improved analysis of the sshi interface in piezoelectric energy harvesting, Smart Materials and Structures 16 (6) (2007) 2253.

[23] E. Lefeuvre, A. Badel, C. Richard, D. Guyomar, Piezoelectric energy harvesting device optimization by synchronous electric charge extraction, Journal of Intelligent Material Systems and Structures 16 (10) (2005) 865–876.

[24] K. Uchino, Piezoelectric Actuators and Ultrasonic Motors, Vol. 1, Kluwer Academic Publisher, 1996.

[25] V. Kulkarni, R. Ben Mrad, S. Prasad, S. Nemana, Assessment of an energy harvester based on shear mode piezoceramics, in: Mechatronics and its Applications (ISMA), 2012 8th International Symposium on, 2012, pp. 1–3.

[26] A. Badel, A. Benayad, E. Lefeuvre, L. LeBrun, C. Richard, D. Guyomar, Single crystals and nonlinear process for outstanding vibration-powered electrical generators, Ultrasonics, Ferroelectrics and Frequency Control, IEEE Transactions on 53 (4) (2006) 673–684.

Biographies

Adrian Z. Amanci received his B.AS. and M.AS.in 2007 and 2009 respectively, from the University of Toronto, Canada, both in electrical engineering. He is currently pursuing a PhD degree in electrical engineering at the University of Toronto under the joint supervision of Professor Francis P. Dawson and Harry E. Ruda. His research interests are piezoelectric power generation, the development of monitoring and control devices for large scale power systems and high frequency passive power devices.

Frédéric Giraud graduated from the Ecole Normale Supérieure de Cachan, France in 1996 in electrical engineering, and received his PhD from the University Lille1, in 2002. He is a member of the electrical engineering and power electronics laboratory of Lille where he works as an Associate Professeur. His research deals with the modelling and the control of piezo-electric actuators.

Christophe Giraud-Audine received his M.Eng. degree in mechanical engineering from the École Nationale Supérieure d'Arts et Métiers in 1992, and his Ph.D degree in electrical engineering from the Institut National Polytechnique de Toulouse in 1998. After two years spent as a Research Associate at the University of Sheffield, he joined an associate professor position at the École Nationale Supérieure d'Arts et Métiers. His current research focuses on the modelling and control of systems actuated by piezoelectric and shape memory alloys.

Michel Amberg has been teaching electronics at the University of Lille, France. He graduated from Ecole Normale Supérieure de Cachan, France in 1981. He has tutored more than a hundred Bachelor Students during their projects in the field of telecommunications,computer science and electronics. He is now research engineer at IRCICA, and works on the electronic design of tactile devices.

Francis Dawson received the B.Sc degree in physics and the B.ASc., M.A.Sc., and Ph.D degrees in electrical engineering from the University of Toronto in 1978, 1982, 1985, and 1988, respectively.

He worked as a process control engineer in the pulp and paper, rubber and textile industries during the period 1978-1980. From 1982 to 1984 he acted as a consultant on various projects. Development areas included high-frequency link power supplies, power supplies for specialized applications and high current protection circuits. Since 1988 he has been with the Department of Electrical and Computer Engineering, University of Toronto where he is engaged in teaching and research.

His areas of research interest include static power converters and their applications, signal processing in power engineering applications, energy storage systems and device or process modeling. He has also participated as a Consultant or Project Leader in several industrial projects. Dr. Dawson is a member of the Association of Professional Engineers of Ontario and is an IEEE Fellow.

Betty Lemaire-Semail (Ph.D'90, University of Paris XI, Orsay). From 1990 to 1998, she was assistant profes-

sor in the Ecole Centrale of Lille and she is now professor at the University Lille1. She is a member of the electrical engineering and power electronics laboratory of Lille and head of the research axis on the control of electrical systems. She has studied electromagnetic motors and her main field of interest now deals with the modelling and control of piezoelectric actuators, for positioning and force feedback applications.

List of Figures